Chapter 6
Holistic Uncertainty Quantification for Dynamic Substructuring in the Frame-wing Problem

Teresa Portone, Benjamin Moldenhauer, and Daniel Roettgen

Abstract Dynamic substructuring enables the assessment of large and complex dynamic systems through the combination of individually analyzed system components. Substructuring can be applied to simulations, experiments, or a hybrid of both and is an effective way to understand the system-level effect of swapping one component in the system for another. Uncertainties arise in experiments, simulations, and the dynamic substructuring process. These uncertainties affect analysis results. To date, uncertainty quantification (UQ) has not been rigorously and holistically applied to dynamic substructuring. We previously quantified simulation and substructuring uncertainties in SEM's frame-wing dynamic substructuring benchmark structure. In this work we additionally integrate experimental measurement uncertainties. We then investigate the relative importance of uncertainties to analysis results, where we vary which aspects of the dynamic substructuring problem are simulation-based or test-based.

Keywords Dynamic Substructuring · Hybrid Modeling · Component Mode Synthesis · Uncertainty Quantification · Sensitivity Analysis

Introduction

Experimental modal analysis transforms a set of measured responses into single degree-of-freedom (DOF) modal responses. Linear modal analysis is a useful tool for updating finite element models, performing low excitation level system predictions, and obtaining modal information about a mechanical system (i.e., natural frequencies and mode shapes). Modal analysis is often the building block for analyzing structural performance of assemblies, but it can be difficult to apply to complex structures, especially jointed structures and/or those with evolving hardware, where not all components are in-hand at time of test.

Dynamic substructuring [1] incorporating the transmission simulator (TS) method [2, 3, 4, 5] enables synthesis of experimental and simulation-based dynamical models of different structures to predict the response of a new structure which couples them together. This has the potential to be a highly powerful engineering tool for answering speculative questions about the impacts of part swap or hardware maturation.

However, the accuracy of predictions for a new structure is influenced by many uncertainties arising from computational models, experiments, and the dynamic substructuring procedure. To date, a holistic assessment of such uncertainties on dynamic substructuring predictions has not been performed. In this work we present a preliminary holistic quantification of these uncertainties for the Dynamic Substructuring SEM Round Robin problem [6].

Teresa Portone
Optimization and Uncertainty Quantification Department
e-mail: tporton@sandia.gov

Benjamin Moldenhauer · Daniel Roettgen
Experimental Structural Dynamics Department
Sandia National Laboratories, Albuquerque, NM 87123
e-mail: bmolden@sandia.gov; drroett@sandia.gov

© The Author(s), under exclusive license to River Publishers 2026

Kristin B. Zimmerman, PhD (eds.), *Dynamic Substructuring & Transfer Path Analysis, 2026, Vol. 4*, Conference Proceedings of the Society for Experimental Mechanics Series, https://doi.org/10.13052/rp-9788743814153

Background

Modal substructuring with transmission simulator

Here we summarize the dynamic substructuring [1] and transmission simulator (TS) methods [2, 3, 4, 5] which we employed in this work. The multi-degree of freedom equations of motion are

$$\mathbf{M}\ddot{\mathbf{x}} + \mathbf{C}\dot{\mathbf{x}} + \mathbf{K}\mathbf{x} = \mathbf{f}, \tag{1}$$

where $\mathbf{M}$, $\mathbf{C}$, and $\mathbf{K}$ are the mass, damping, and stiffness matrices, respectively, $\mathbf{f}$ is the external excitation (forcing), and $\mathbf{x}$ is the vector of physical displacements at tracked physical degrees of freedom. For lightly damped systems, mode shapes are found by solving a generalized eigenproblem, where the mode shape vectors are the eigenvectors of the undamped oscillator under null excitation, and the squares of modal frequencies are the eigenvalues:

$$(\mathbf{K} - \omega_i^2 \mathbf{M})\phi_i = 0, \quad i = 1, \ldots, N. \tag{2}$$

For systems with well-separated modal frequencies, mass-normalized mode shapes simultaneously diagonalize the mass and stiffness matrices.

This equation can be transformed into modal coordinates by setting

$$\mathbf{x} = \mathbf{\Phi}\mathbf{q}, \tag{3}$$

where $\mathbf{q}$ are the modal coordinates and $\mathbf{\Phi} \in \mathbb{R}^{N_p \times N}$ is the modal matrix with columns consisting of the mass-normalized mode shape vectors, where N_p is the number of physical coordinates $\mathbf{x}$ and N is the number of modal degrees of freedom.

The system can be diagonalized by premultiplying by $\mathbf{\Phi}^T$:

$$\mathbf{\Phi}^T\mathbf{M}\mathbf{\Phi}\ddot{\mathbf{q}} + \mathbf{\Phi}^T\mathbf{C}\mathbf{\Phi}\dot{\mathbf{q}} + \mathbf{\Phi}^T\mathbf{K}\mathbf{\Phi}\mathbf{q} = \mathbf{\Phi}^T\mathbf{f}. \tag{4}$$

Assuming the properties of well-separated modal frequencies and lightly damped systems hold, the system is thus diagonalized and can be written as

$$\mathbf{I}\ddot{\mathbf{q}} + 2\zeta\omega\dot{\mathbf{q}} + \omega^2\mathbf{q} = \tilde{\mathbf{f}} \tag{5}$$

Let us now assume we want to couple two subsystems A and B using modal substructuring. In the primal (as opposed to dual) approach to substructuring, their equations of motion can be concatenated as

$$\begin{bmatrix} \mathbf{I_A} & \mathbf{0} \\ \mathbf{0} & \mathbf{I_B} \end{bmatrix} \begin{bmatrix} \ddot{\mathbf{q}}_\mathbf{A} \\ \ddot{\mathbf{q}}_\mathbf{B} \end{bmatrix} + \begin{bmatrix} 2\zeta_A\omega_A & \mathbf{0} \\ \mathbf{0} & 2\zeta_B\omega_B \end{bmatrix} \begin{bmatrix} \dot{\mathbf{q}}_\mathbf{A} \\ \dot{\mathbf{q}}_\mathbf{B} \end{bmatrix} + \begin{bmatrix} \omega_A^2 & \mathbf{0} \\ \mathbf{0} & \omega_B^2 \end{bmatrix} \begin{bmatrix} \mathbf{q_A} \\ \mathbf{q_B} \end{bmatrix} = \begin{bmatrix} \tilde{\mathbf{f}}_\mathbf{A} \\ \tilde{\mathbf{f}}_\mathbf{B} \end{bmatrix}, \tag{6}$$

$$\begin{bmatrix} \mathbf{x_A} \\ \mathbf{x_B} \end{bmatrix} = \begin{bmatrix} \mathbf{\Phi}_A & \mathbf{0} \\ \mathbf{0} & \mathbf{\Phi}_B \end{bmatrix} \begin{bmatrix} \mathbf{q_A} \\ \mathbf{q_B} \end{bmatrix}, \tag{7}$$

where $\mathbf{\Phi}_A \in \mathbb{R}^{N_p^A \times N_A}$ and $\mathbf{\Phi}_B \in \mathbb{R}^{N_p^B \times N_B}$.

In the primal substructuring approach, physical degrees of freedom are coupled between the subsystems at their interface, to enforce the same motion in each subsystem at that location. Let the projection of the full set of physical coordinates to the constraint coordinates be denoted $\mathbf{P_A^c} \in \mathbb{R}^{N_c \times N_p^A}$ for subsystem A and $\mathbf{P_B^c} \in \mathbb{R}^{N_c \times N_p^B}$ for subsystem B. Similarly, let the set of physical coordinates to be constrained be denoted $\mathbf{x_A^c}$ and $\mathbf{x_B^c}$. Then

$$\mathbf{x_A^c} = \mathbf{P_A^c}\mathbf{x_A} \qquad \mathbf{x_B^c} = \mathbf{P_B^c}\mathbf{x_B} \tag{8}$$

and

$$\begin{bmatrix} \mathbf{I} & -\mathbf{I} \end{bmatrix} \begin{bmatrix} \mathbf{P_A^c}\mathbf{x_A} \\ \mathbf{P_B^c}\mathbf{x_B} \end{bmatrix} = \mathbf{0}, \tag{9}$$

where $\mathbf{I} \in \mathbb{R}^{N_c \times N_c}$ and $\mathbf{0} \in \mathbb{R}^{N_c}$.

Translating these constraints to modal coordinates, we can define the mode shapes at the subset of constraint coordinates as $\mathbf{\Phi}^c = \mathbf{P^c}\mathbf{\Phi} \in \mathbb{R}^{N_c \times N}$. Then

$$\begin{bmatrix} \mathbf{I} & -\mathbf{I} \end{bmatrix} \begin{bmatrix} \mathbf{\Phi}_A^c\mathbf{q_A} \\ \mathbf{\Phi}_B^c\mathbf{q_B} \end{bmatrix} = \mathbf{0}, \tag{10}$$

or, equivalently,

$$\begin{bmatrix}\boldsymbol{\Phi}_A^c & -\boldsymbol{\Phi}_B^c\end{bmatrix}\begin{bmatrix}\mathbf{q_A}\\ \mathbf{q_B}\end{bmatrix} = \mathbf{B}\begin{bmatrix}\mathbf{q_A}\\ \mathbf{q_B}\end{bmatrix} = \mathbf{0}. \tag{11}$$

When there are multiple constraint points, numerically it can be very challenging to exactly satisfy the equality of motions at the interface. Additionally, when experimental data is used for one or both of the subsystems, it can be impossible to exactly satisfy the above equality. The transmission simulator approach can alleviate the former challenge, while constraint softening can alleviate the latter.

Solving the equations of motion coupled to the constraint equations would be challenging because the constraints are not satisfied for arbitrary values of $\mathbf{q_A}$ and $\mathbf{q_B}$. Instead, we seek a transformation from a generalized set of coordinates to our modal coordinates, such that the constraints are automatically satisfied for arbitrary values of the generalized coordinates. The generalized coordinates are the coordinates of the assembled system (the combined system after all constraints are enforced). These generalized coordinates $\boldsymbol{\eta}$ are defined such that

$$\begin{bmatrix}\mathbf{q_A}\\ \mathbf{q_B}\end{bmatrix} = \mathbf{L}\boldsymbol{\eta}. \tag{12}$$

Substituting this expression into the compatibility condition (the constraint system) above, we want

$$\mathbf{BL}\boldsymbol{\eta} = \mathbf{0}. \tag{13}$$

Since we want this relationship to hold for any arbitrary value of $\boldsymbol{\eta}$, we require that $\mathbf{L}$ span the nullspace of $\mathbf{B}$. The dimension of the nullspace of $\mathbf{B}$ thus determines the dimensions of $\mathbf{L}$ and $\boldsymbol{\eta}$.

Substituting the equation for the generalized coordinates into the combined modal equations of motion for the subsystem and premultiplying by $\mathbf{L}^T$, we obtain the coupled system of equations

$$\mathbf{L}^T\begin{bmatrix}\mathbf{I_A} & \mathbf{0}\\ \mathbf{0} & \mathbf{I_B}\end{bmatrix}\mathbf{L}\ddot{\boldsymbol{\eta}} + \mathbf{L}^T\begin{bmatrix}2\zeta_A\omega_A & \mathbf{0}\\ \mathbf{0} & 2\zeta_B\omega_B\end{bmatrix}\mathbf{L}\dot{\boldsymbol{\eta}} + \mathbf{L}^T\begin{bmatrix}\omega_A^2 & \mathbf{0}\\ \mathbf{0} & \omega_B^2\end{bmatrix}\mathbf{L}\boldsymbol{\eta} = \mathbf{L}^T\begin{bmatrix}\tilde{\mathbf{f}}_\mathbf{A}\\ \tilde{\mathbf{f}}_\mathbf{B}\end{bmatrix}, \tag{14}$$

or, in condensed notation,

$$\hat{\mathbf{M}}\ddot{\boldsymbol{\eta}} + \hat{\mathbf{C}}\dot{\boldsymbol{\eta}} + \hat{\mathbf{K}}\boldsymbol{\eta} = \hat{\mathbf{f}} \tag{15}$$

Since N_c constraints are enforced, the coupled system will only have $(N_A + N_B) - N_c$ degrees of freedom. The mode shapes of the assembled (coupled) system can then be computed by solving the generalized eigenvalue problem with $\hat{\mathbf{M}}$ and $\hat{\mathbf{K}}$.

As previously mentioned, exactly satisfying the constraints $\mathbf{B}$ can be numerically challenging. The transmission simulator (TS) approach alleviates these challenges by mass-loading the interface between two subsystems. The TS approach augments the set of equations from the standard modal substructuring approach between two subsystems A and B with another set of equations for the so-called TS, which is typically a component in one of the subsystems. Let's assume the TS is a component of the subsystem A. A negative form of the component is coupled to the equations of motion for A and B:

$$\begin{aligned}&\begin{bmatrix}\mathbf{I_A} & \mathbf{0} & \mathbf{0}\\ \mathbf{0} & \mathbf{I}_B & \mathbf{0}\\ \mathbf{0} & \mathbf{0} & -\mathbf{I}_{TS}\end{bmatrix}\begin{bmatrix}\ddot{\mathbf{q}}_\mathbf{A}\\ \ddot{\mathbf{q}}_\mathbf{B}\\ \ddot{\mathbf{q}}_\mathbf{TS}\end{bmatrix} + \begin{bmatrix}2\zeta_A\omega_A & \mathbf{0} & \mathbf{0}\\ \mathbf{0} & 2\zeta_B\omega_B & \mathbf{0}\\ \mathbf{0} & \mathbf{0} & -2\zeta_{TS}\omega_{TS}\end{bmatrix}\begin{bmatrix}\dot{\mathbf{q}}_\mathbf{A}\\ \dot{\mathbf{q}}_\mathbf{B}\\ \dot{\mathbf{q}}_\mathbf{TS}\end{bmatrix} + \dots\\ &\qquad\qquad \cdots + \begin{bmatrix}\omega_A^2 & \mathbf{0} & \mathbf{0}\\ \mathbf{0} & \omega_B^2 & \mathbf{0}\\ \mathbf{0} & \mathbf{0} & -\omega_{TS}^2\end{bmatrix}\begin{bmatrix}\mathbf{q_A}\\ \mathbf{q_B}\\ \mathbf{q_{TS}}\end{bmatrix} = \begin{bmatrix}\tilde{\mathbf{f}}_\mathbf{A}\\ \tilde{\mathbf{f}}_\mathbf{B}\\ \tilde{\mathbf{f}}_\mathbf{TS}\end{bmatrix},\end{aligned} \tag{16}$$

$$\begin{bmatrix}\mathbf{x_A}\\ \mathbf{x_B}\\ \mathbf{x_{TS}}\end{bmatrix} = \begin{bmatrix}\boldsymbol{\Phi}_A & \mathbf{0} & \mathbf{0}\\ \mathbf{0} & \boldsymbol{\Phi}_B & \mathbf{0}\\ \mathbf{0} & \mathbf{0} & \boldsymbol{\Phi}_{TS}\end{bmatrix}\begin{bmatrix}\mathbf{q_A}\\ \mathbf{q_B}\\ \mathbf{q_{TS}}\end{bmatrix}. \tag{17}$$

Note that in general the bottom row should be multiplied by the number of TS components that need to be removed to achieve the desired assembled system. That is, if the TS was also a component of subsystem $\mathbf{B}$ but was not present in the assembled system, we would want to multiply the bottom row of the above equations by 2 (instead of 1).

Instead of coupling physical coordinates directly between A and B, they are now connected to coordinates of the TS. Since we now have two sets of constraints, we can choose to apply the constraints at two different sets of physical locations.

This is sometimes advantageous (and necessary) to remove the motion of the TS from the assembled system. Denoting the first set of constraint coordinates c_A and the second c_B, the constraint (compatibility) equations are

$$\begin{bmatrix} \mathbf{P}_{\mathbf{A}}^{\mathbf{c_A}} & \mathbf{0} & -\mathbf{P}_{\mathbf{TS}}^{\mathbf{c_A}} \\ \mathbf{0} & \mathbf{P}_{\mathbf{B}}^{\mathbf{c_B}} & -\mathbf{P}_{\mathbf{TS}}^{\mathbf{c_B}} \end{bmatrix} \begin{bmatrix} \mathbf{x_A} \\ \mathbf{x_B} \\ \mathbf{x_{TS}} \end{bmatrix} = \begin{bmatrix} \mathbf{0} \\ \mathbf{0} \end{bmatrix}, \tag{18}$$

or, in terms of modal degrees of freedom,

$$\begin{bmatrix} \boldsymbol{\Phi}_A^{c_A} & \mathbf{0} & -\boldsymbol{\Phi}_{TS}^{c_A} \\ \mathbf{0} & \boldsymbol{\Phi}_B^{c_B} & -\boldsymbol{\Phi}_{TS}^{c_B} \end{bmatrix} \begin{bmatrix} \mathbf{q_A} \\ \mathbf{q_B} \\ \mathbf{q_{TS}} \end{bmatrix} = \mathbf{B} \begin{bmatrix} \mathbf{q_A} \\ \mathbf{q_B} \\ \mathbf{q_{TS}} \end{bmatrix} = \begin{bmatrix} \mathbf{0} \\ \mathbf{0} \end{bmatrix}. \tag{19}$$

In most practical use cases, e.g., using experimental data for one of the subsystems, there are many challenges that mitigate the ability to exactly satisfy these constraints. There is noise in the experiments, the degrees of freedom are not exactly coincident, and modes are truncated due to finite measurement capabilities. Therefore it is necessary to soften the constraints, which we do in this work using the pseudoinverse of the TS shape matrix projected down to constraint locations.

Note that since the constraint locations may differ along the row-blocks of the matrix (19), the pseudoinverse is constructed and applied for each set of constraints individually. This results in two constraint-softening matrices $\left(\boldsymbol{\Phi}_{TS}^{c_A}\right)^{\dagger}$ and $\left(\boldsymbol{\Phi}_{TS}^{c_B}\right)^{\dagger}$ for the sets of constraints coupling the TS motion to subsystems A and B respectively:

$$\begin{bmatrix} \left(\boldsymbol{\Phi}_{TS}^{c_A}\right)^{\dagger} & \mathbf{0} \\ \mathbf{0} & \left(\boldsymbol{\Phi}_{TS}^{c_B}\right)^{\dagger} \end{bmatrix} \begin{bmatrix} \boldsymbol{\Phi}_A^{c_A} & \mathbf{0} & -\boldsymbol{\Phi}_{TS}^{c_A} \\ \mathbf{0} & \boldsymbol{\Phi}_B^{c_B} & -\boldsymbol{\Phi}_{TS}^{c_B} \end{bmatrix} \begin{bmatrix} \mathbf{q_A} \\ \mathbf{q_B} \\ \mathbf{q_{TS}} \end{bmatrix} = \mathbf{B} \begin{bmatrix} \mathbf{q_A} \\ \mathbf{q_B} \\ \mathbf{q_{TS}} \end{bmatrix} = \begin{bmatrix} \mathbf{0} \\ \mathbf{0} \end{bmatrix}. \tag{20}$$

Having defined **B** for this system of equations (including constraint softening), the solution then proceeds as before from (12).

Uncertainty Quantification

There are many potential sources of uncertainty in this workflow: measurement uncertainties, computational model uncertainties, and substructuring uncertainties. A (nonexhaustive) list of these potential sources is presented in Table 1.

Table 1 Sources of uncertainty for different aspects of the dynamic substructuring problem.

Computational model uncertainty	Measurement uncertainty	Substructuring uncertainty
	• Instrumentation selection	
• Geometry	• Modal truncation	• Mode selection
• Material properties	• Person-to-person variability	• Constraint DOF selection
• Joint model	• Unit-to-unit variability	• Constraint softening
	• Measurement error	

The aim of this work is to make a preliminary, holistic characterization of these uncertainties for the Dynamic Substructuring SEM Round Robin problem and to measure which sources of uncertainty are most influential to predicted quantities of interest (QoIs) such as mode shapes and natural frequencies of the target structure of interest. This is done by representing sources of uncertainty as random variables and propagating samples of these uncertainties through the dynamic substructuring workflow to predicted QoIs. These samples can then be used to compute statistical information about the QoIs and the relative influence of the uncertainty sources.

Variance-based sensitivity analysis in the form of Sobol' indices is a key method to measure the influence of inputs on predicted outputs [7, 8]. Sobol' indices measure the fraction of variance in predicted QoIs that can be attributed to a given input factor, with a larger index corresponding to a more influential input. Main effects indices measure the fraction of variance attributed to a given input alone, while total effects indices measure the fraction of variance attributed to an input along with its interactions with other inputs (e.g., the influence of two inputs varying together on an output).

Input factors for Sobol' indices may be individual parameters or groups of parameters. In this work we focus on groups of parameters aggregated according to the type of uncertainty they represent—measurement, computational model, or substructuring. Under the assumption of independent inputs, Sobol' indices (being fractions of total output variance) fall in the range $[0, 1]$. The influence of input factors can be ranked in order of importance by their Sobol' index values.

Sobol' indices and other sample statistics like the mean and variance of a QoI are computed using random input-output samples, so they exhibit statistical variation for finite sample size. Due to numerical conditioning challenges in the substructuring when randomly sampling the number of modes, we are able to attain relatively few ($\sim$300) random input-output samples with which to compute our statistics, while typically Sobol' indices are computed with several thousand samples at a minimum. Therefore, we use the bootstrap method to approximate the statistical variation in our estimates [9].

The bootstrap sampling method repeatedly resamples our input-output sample set and computes statistics for each resampled set. Bootstrap resamples with replacement, meaning it draws N random samples from the original size-N sample set, allowing the same sample point to be picked more than once (picture drawing a random card, placing it back in the deck, shuffling, then drawing a card again). The intuition behind this approach is that (provided you have enough samples to start with) your sample set approximates the probability distribution it was drawn from. Thus these resampled sets approximate the samples you would get if you could repeatedly sample the underlying probability distribution. By computing sample statistics for each of these resampled sets, we can measure how much our statistical estimates could vary if we had gathered many different samples from the probability distribution. This lets us measure our confidence in the computed statistics, e.g., by computing confidence bounds over the bootstrap sample.

Analysis

In this work we investigate the relative influence of measurement, simulation, and substructuring uncertainties on dynamic substructuring predictions in the context of the Dynamic Substructuring SEM Round Robin problem, called herein the frame-wing problem [6]. A diagram of the specific case we consider is shown in Figure 1. We assume a baseline structure of a frame attached to a thin wing, and we use dynamic substructuring to predict the dynamic response of a target structure where the thin wing is swapped for a thick wing. We use Sierra/SD [10] for all finite-element model (FEM) computations and SDynPy (https://sandialabs.github.io/sdynpy/) for all dynamic substructuring computations.

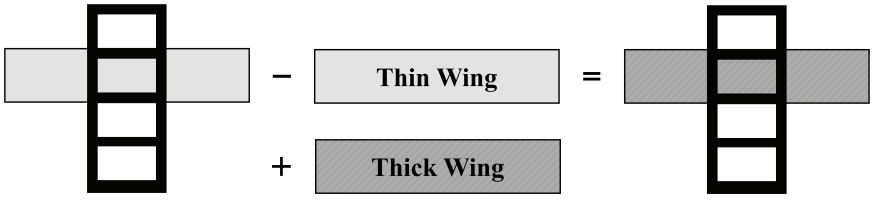

Fig. 1 A diagram of the targeted dynamic substructuring problem. The baseline structure is the thin wing bolted to the frame. We will remove the thin wing and substructure in the thick wing using the approach described in the background section.

Of particular interest is whether the most influential uncertainties to dynamic substructuring predictions change depending on which modal models arise from test or simulation. To study this question, we consider two cases, depicted in Figure 2. In the "simulation baseline" case, the baseline structure's modal model is assumed to arise from a simulation and the wing modal models are assumed to arise from tests. In the "test baseline" case, this is reversed—the baseline structure modal model is assumed to arise from a test and the wing modal models are assumed to arise from simulations. In all cases, each modal model is *in actuality* computed from a finite-element model (FEM), but either the FEM or the modal model is perturbed to reflect the type of uncertainties associated with it. For example, for a modal model assumed to arise from test we perturb its damping ratios and natural frequencies from their nominal values, with a much more significant perturbation of damping ratios than of natural frequencies in order to mimic the degree of uncertainty in these quantities when they are derived from test.

Uncertainty characterization

For simulation-based uncertainties we consider a subset of all the possible uncertainties that could arise. These uncertainties are defined in Table 2. Additional uncertainties besides those in Table 2 that could be influential in these types of studies

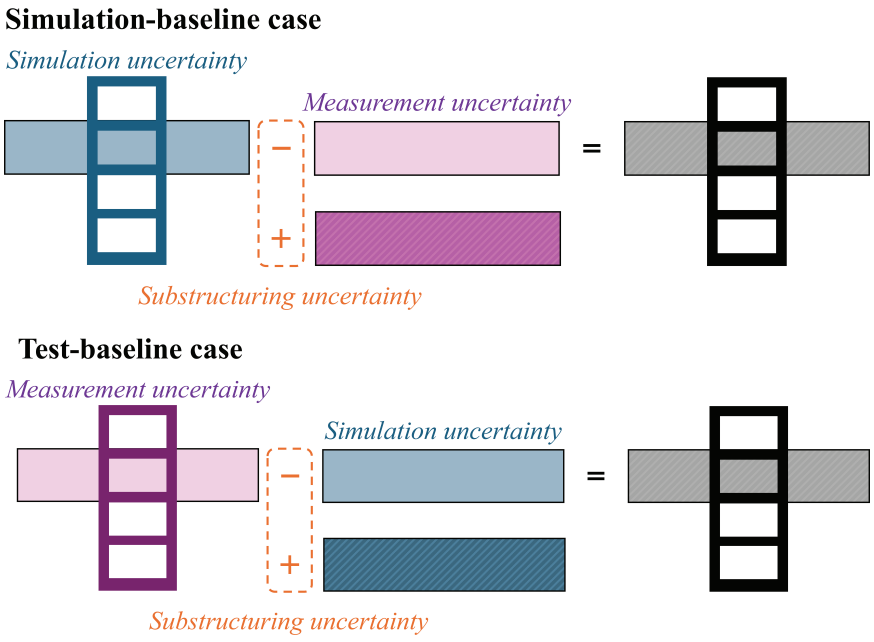

Fig. 2 A diagram of the two cases that introduce different types of uncertainty into the dynamic substructuring problem in different places.

are geometric uncertainty (e.g., lack of information about as-manufactured parts), contact model uncertainty (varying the type of contact model if the most suitable approach is unknown), and heterogeneous uncertainties (e.g., spatially-varying material properties, individually varying contact uncertainties). Incorporation of such uncertainties is left to future work. Note that joint model uncertainties are only incorporated in the simulation-baseline case since joint behavior is captured in the test-based modal model for the test-baseline case.

Table 2 Computational model uncertainties considered herein.

Uncertainty type	Uncertain input	Probability distribution
Material properties	Young's moduli $E_{frame}, E_{thin}, E_{thick}$ [GPa]	$\mathscr{U}[60, 80]$
	Densities $\rho_{frame}, \rho_{thin}, \rho_{thick}$ [kg/m^3]	$\mathscr{U}[2650, 2800]$
Bolted joint model	Joint bolt and washer mass m_{bw} [kg]	$\mathscr{U}[3.14, 4.71] \cdot 10^{-3}$ *nominal* $\pm 20\%$
	Translational spring constants k_t [N/m]	$\log \mathscr{U}[1.5 \cdot 10^7, 1.5 \cdot 10^9]$ *nominal* ± 1 *order of magnitude*
	Rotational spring constants k_r [N/m]	$\log \mathscr{U}[10^6, 10^8]$ *nominal* ± 1 *order of magnitude*

To quantify measurement uncertainty we pose probability distributions for perturbations to the modal model based on the study performed in [11], wherein 17 experimentalists performed hammer tests on a similar frame-wing structure. Since the structure was not identical to the one considered here we can't directly sample from the data, but since the structure is similar, we expect the uncertainties to exhibit similar behavior. Therefore, we used the data to define plausible perturbations to the nominal modal model. Specifically, we generated empirical distributions of the probable percent difference from the mean value for natural frequencies and damping ratios, which are depicted in Figure 3. It was observed in [11] that there was not significant variation in the mode shapes, at least as measured by the modal assurance criterion, so they were not varied in this study.

We additionally imposed correlations between the perturbations, since it was observed that, in general, natural frequencies were positively correlated amongst themselves (i.e., if a test-based modal model's first natural frequency was lower than the mean, all the natural frequencies were lower than the mean), as were the damping ratios. However, there was a negative correlation between the natural frequencies and the damping ratios (if natural frequencies were lower than the mean, damping ratios were greater, and vice versa). This behavior is likely due to the presence of bolted joints in the test assembly, as the

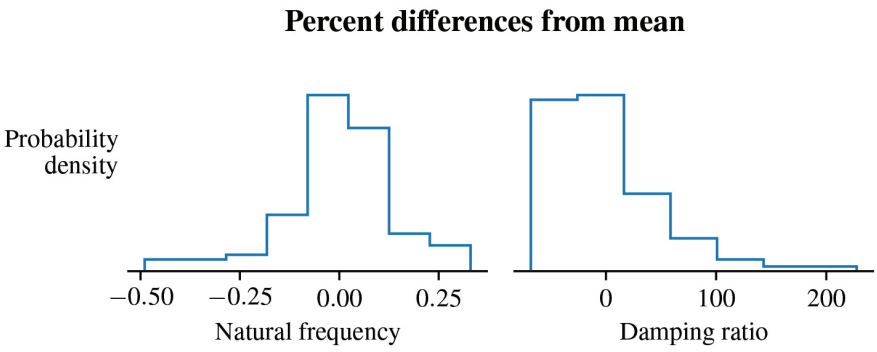

Fig. 3 Histograms of percent differences from mean values for natural frequencies and damping ratios, computed over the 17 datasets and including percent differences for all modes in the test-based modal models. The damping ratios can exhibit deviations up to 200% from the mean, while natural frequencies exhibit small deviations of less than 1%.

effective nonlinear dynamic properties of jointed structures typically display decreasing natural frequencies and increasing damping ratios [12]. We defined the correlation matrix used herein by computing the average (over the 17 datasets) positive correlation between natural frequencies, the average positive correlation between damping ratios, and the average negative correlation between frequencies and damping ratios. These average correlations were applied in a block-wise fashion to the correlation matrix we used to sample perturbations. The correlation matrix is shown in Figure 4.

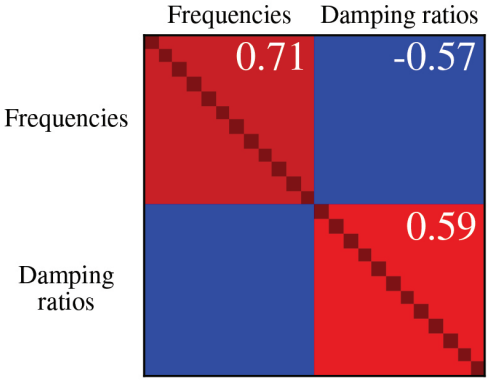

Fig. 4 The block-defined correlation matrix imposed between all frequency and damping ratio perturbations. The constant values assigned in each block are noted in the block; the matrix is symmetric. The diagonal is equal to 1 by definition.

The perturbations were sampled and applied to simulate measurement uncertainty as follows. The percent differences in frequencies (ω_{pd}) and damping ratios (ζ_{pd}) are sampled jointly according to their empirical distributions, subject to the correlations specified above. They are then applied to the nominal values ω_n and ζ_n to obtain sample values ω_s and ζ_s as

$$\omega_s = \omega_n \cdot \left(1 + \frac{\omega_{pd}}{100}\right), \qquad \zeta_s = \zeta_n \cdot \left(1 + \frac{\zeta_{pd}}{100}\right).$$

These perturbations were applied either to the baseline structure for the "test baseline" case, or to the wings, in the "simulation baseline" case. It is possible that the measurement uncertainties for the frame-wing structure are not appropriate for the wings alone, as the wing alone does not contain any bolted interfaces that would introduce significant variance in the dynamic properties due to nonlinear behavior. However, we leave such investigations to future work.

Finally, our preliminary quantification of substructuring uncertainty focuses on the number of modes from each subsystem to include. In this case we randomly sample within a range for each of the subsystems. The sampling structure is depicted in Figure 5. To define the range for the baseline structure, we identify the lowest mode above 1600 Hz, so that the substructured system has modes up to at least that many Hz. We then randomly sample the number of modes for the baseline system between this lowest mode and 50 modes, the total number of modes in our set. For the wings, we know we want to have at least one flexible mode included in substructuring, so we set the first flexible mode as our lower bound, and we don't want to include more modes than were taken from the baseline structure. We therefore randomly sample the number of modes between the first flexible mode and the number of modes from the baseline structure.

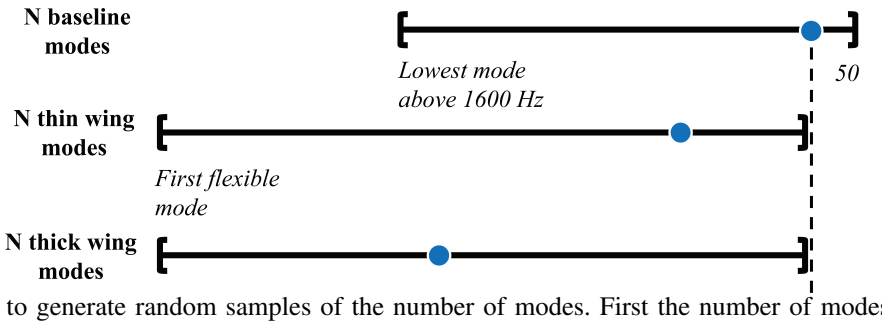

Fig. 5 The scheme to generate random samples of the number of modes. First the number of modes from the baseline structure is sampled; this is used to set an upper bound for the number of modes for each of the wings.

Quantities of Interest (QoIs)

We consider two key dynamic QoIs in this work: the accuracy of the substructured natural frequencies, and the accuracy of the substructured mode shapes. Accuracy of damping ratios is left to future work. To measure accuracy we compare the substructured values to the values derived from an updated model of the target structure, the frame and thick wing assembly, which we call here the "truth" system. Our quantity of interest for the natural frequencies is computed as follows. We identify the nearest unique natural frequency in the truth system to the first 10 natural frequencies in the substructured system (this is to cover the case where a mode is missing in the substructured system). We then compute the relative error for each of these first 10 natural frequencies relative to the truth value and compute the average over the 10 natural frequencies. To measure mode-shape accuracy we count how many substructured modes have a high MAC score (at least 0.85) with a single mode shape in the truth system.

Sensitivity Analysis

In Figure 6 we present the Sobol' sensitivity indices for our two QoIs, for our two baseline cases. As discussed in the background section on uncertainty quantification, the indices are presented as distributions of values generated from bootstrap

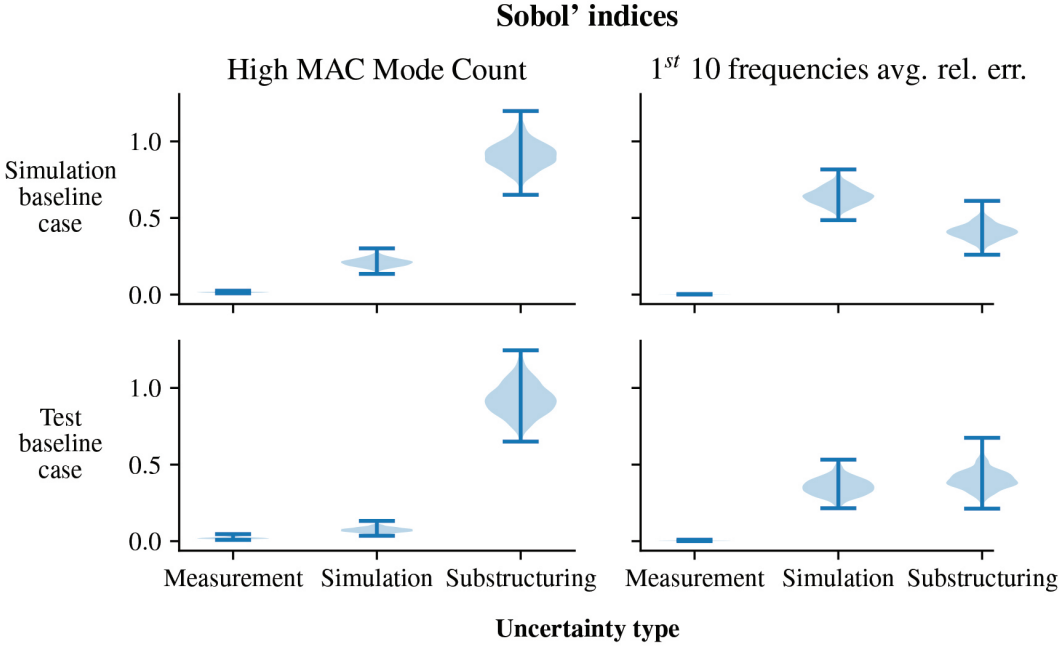

Fig. 6 Violin plots for the Sobol' indices attributed to each source of uncertainty in the dynamic substructuring problem for the simulation baseline case and the test baseline case. The shaded regions in the violin plots show the distribution of values over a sample set—in this case, that set is the set of bootstrap samples we generated to estimate the variability in our index estimates. The horizontal bars indicate the maximum and minimum value achieved over the set.

to represent the possible variability in their values due to using a finite set of samples for their estimation. For all cases and QoIs the substructuring uncertainty's sensitivity index takes a significant nonzero value, making it clear that it is an important source of uncertainty. The simulation uncertainty's sensitivity index ranges are higher for the simulation baseline case than the test baseline case for both QoIs. This makes sense since the joint modeling uncertainty is only included in the simulation baseline case.

Additionally, it is more influential for natural frequency accuracy than mode shape accuracy as the frequency comparison is operating directly on scalar values, while the MAC is more of an averaged metric over all degrees of freedom in the mode shape. Finally, measurement uncertainty's index is very close to zero in all cases, indicating it is not important for any baseline case or QoI. Since the greatest measurement uncertainty manifests in the damping ratios, which weren't considered as a QoI here, this is not necessarily surprising.

Conclusion

In this work, we performed a preliminary holistic quantification and identification of important uncertainties in dynamic substructuring in the context of the SEM Frame-Wing Round Robin challenge problem. We considered two cases to assess the importance of different sources of uncertainty: one case where the baseline structure's modal model is assumed to arise from test, and one case where it is assumed to arise from simulation. We quantified uncertainties from simulations, test, and substructuring.

Our results indicate that substructuring uncertainties were the dominant source of uncertainty for this dynamic substructuring problem. More rigorous methods to define reasonable (tighter) bounds on the number of modes to include from each subsystem would help drive this uncertainty down. However, there are several limitations to the current study that should be addressed to draw any general conclusions about the most important source of uncertainty in such problems. First, a broader set of quantities of interest should be examined; for example, the damping ratios of the substructured system will be the subject of future work. Additionally, considering uncertainties in dynamic substructuring for other structures will be critical to identifying trends (or lack thereof) in which uncertainties are most important.

Acknowledgments This article has been authored by an employee of National Technology & Engineering Solutions of Sandia, LLC under Contract No. DE-NA0003525 with the U.S. Department of Energy (DOE). The employee owns all right, title and interest in and to the article and is solely responsible for its contents. The United States Government retains and the publisher, by accepting the article for publication, acknowledges that the United States Government retains a non-exclusive, paid-up, irrevocable, world-wide license to publish or reproduce the published form of this article or allow others to do so, for United States Government purposes. The DOE will provide public access to these results of federally sponsored research in accordance with the DOE Public Access Plan https://www.energy.gov/downloads/doe-public-access-plan. This paper describes objective technical results and analysis. Any subjective views or opinions that might be expressed in the paper do not necessarily represent the views of the U.S. Department of Energy or the United States Government.

References

1. de Klerk, D., Rixen, D.J., and Voormeeren, S.N., "General Framework for Dynamic Substructuring: History, Review and Classification of Techniques". *AIAA Journal*, 46(5):1169–1181 (2008).
2. Mayes, R.L. and Arviso, M., "Design studies for the transmission simulator method of experimental dynamic substructuring" (2010).
3. Mayes, R.L., Allen, M.S., and Kammer, D.C., "Eliminating Indefinite Mass Matrices with the Transmission Simulator Method of Substructuring". In Mayes, R., Rixen, D., Griffith, D., De Klerk, D., Chauhan, S., Voormeeren, S., and Allen, M., editors, *Topics in Experimental Dynamics Substructuring and Wind Turbine Dynamics, Volume 2*, pages 21–31, Springer, New York (2012).
4. Allen, M.S., Mayes, R.L., and Bergman, E.J., "Experimental modal substructuring to couple and uncouple substructures with flexible fixtures and multi-point connections". *Journal of Sound and Vibration*, 329(23):4891–4906 (2010).
5. Allen, M.S., Gindlin, H.M., and Mayes, R.L., "Experimental modal substructuring to estimate fixed-base modes from tests on a flexible fixture". *Journal of Sound and Vibration*, 330(18):4413–4428 (2011).
6. Roettgen, D.R., Linderholt, A., and Moldenhauer, B.J., "Technical Division Benchmark Structure for Dynamic Substructuring". Orlando, FL (2022).
7. Saltelli, A., "Making best use of model evaluations to compute sensitivity indices". *Computer Physics Communications*, 145(2):280–297 (2002).
8. Prieur, C. and Tarantola, S., "Variance-Based Sensitivity Analysis: Theory and Estimation Algorithms". In Ghanem, R., Higdon, D., and Owhadi, H., editors, *Handbook of Uncertainty Quantification*, pages 1217–1239, Springer, Cham (2017).

9. Chernick, M.R., *Bootstrap Methods: A Guide for Practitioner and Researchers*. Wiley Series in Probability and Statistics, 2nd edition (2008).
10. Bunting, G., Chen, M., Crane, N., Day, D., Dohrmann, C., Hardesty, S., Joffe, D., Lindsay, P., Fliceck, R., and Munday, L., "Sierra/SD-Theory Manual-5.2". Technical report, Sandia National Laboratories (2021).
11. Nguyen, P.C., Roettgen, D.R., and Moldenhauer, B.J., "Uncertainty Quantification in Experimental Modal Analysis". In *Proceedings of the 34th Aerospace Testing Seminar*, Los Angeles, CA, USA (2025).
12. Brake, M.R., "The mechanics of jointed structures: recent research and open challenges for developing predictive models for structural dynamics". Springer (2017).